CHAPTER 6

SUGGESTION FOR FURTHER WORK

(1) The flexibility and stress of single mitered pipe bend is obtained hereto under combined in-plane bending and internal pressure. If possible, a study of single mitered pipe bend under combined out-of-plane bending with internal pressure should have been attempted to observe further phenomena.

(2) The experiment ought to be duplicated with the pipe of larger diameter, thinner pipe wall with longer pipe length. In addition, it is interesting to investigate the variation of stress around the inside surface and compare it with the result obtained herein.

(3) If high pressure equipment is available, it is constructive to conduct the experiment on single mitered pipe bend with higher internal pressure than this in order to extend the experimental study.

(4) In this experiment, the specimen is tested within the range of elastic limit. If condition prevails, the specimen should be loaded until the stress is beyond elastic limit to yield further information.

Appendix I

Basic Equations and Theoretical Development

Assumptions of Theory

1. The theory is that of thin shells, wherein the wall thickness is assumed small compared to the radius of curvature.
2. The theory assumes that the ratio R/r is large compared to unity.
3. It is assumed that the curved pipe or elbow cross-section is initially round.

The effect of internal pressure can be obtained by a relatively simple extension of the energy methods used by von Karman and Vigness (21). Accordingly, we start with the basic energy equations developed by these authors.

$$U_1 = \frac{rtE}{2R^2}\left\{\int_0^{2\pi}\left(\frac{r\Delta\alpha}{\alpha}\sin\phi + w_t\cos\phi + w_r\sin\phi\right)^2 d\phi + \frac{t^2R^2}{12r^4(1-\nu^2)}\int_0^{2\pi}\left(\frac{d^3w_t}{d\phi^3} + \frac{dw_t}{d\phi}\right)^2 d\phi\right\} \quad (1)$$

Equation (1) gives the elastic energy stored in a unit center - line length of curved pipe due to tangential displacements w_t and radial displacements w_r. The assumption made for in-plane bending is

$$w_t = \sum_{n=1}^{\infty} a_n \sin 2n\phi \quad (2)$$

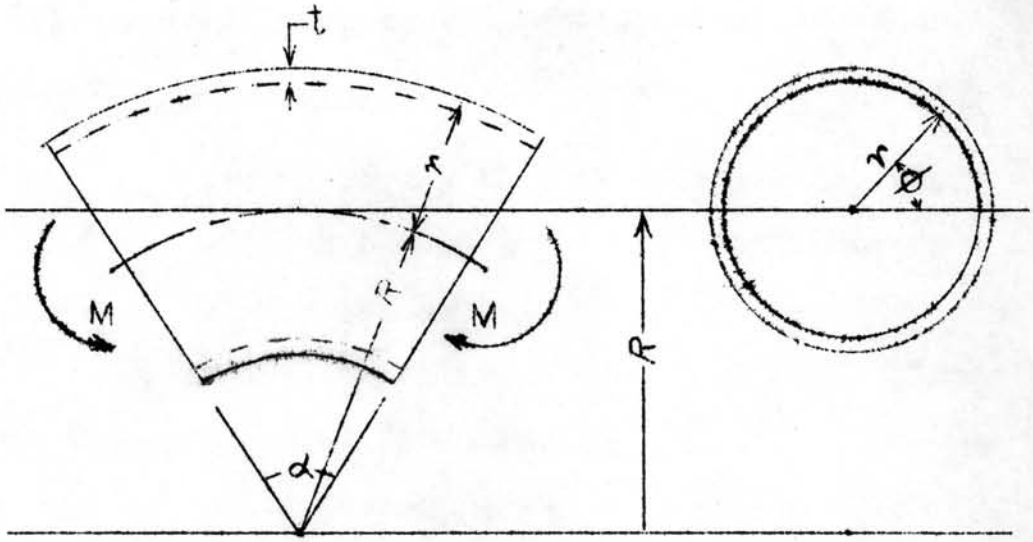

Fig. I-1 Details of the analysis

With the further assumption of inextensibility in the transverse direction, which implies that $w_r = -dw_t / d\phi$, and substituting the trigonometric series expressions for w_t, Equation (1) becomes

$$U_1 = \frac{rtE}{2R^2} \left\{ \int_0^{2\pi} \left(\frac{r\Delta\alpha}{\alpha} \sin\phi + \cos\phi \sum_{n=1}^{\infty} a_n \sin 2n\phi \right. \right.$$
$$\left. - \sin\phi \sum_{n=1}^{\infty} 2na_n \cos 2n\phi \right)^2 d\phi + \frac{\lambda^2}{12} \int_0^{2\pi} \left(-\sum_{n=1}^{\infty} 8n^3 a_n \right.$$
$$\left. \left. \cos 2n\phi + \sum_{n=1}^{\infty} 2na_n \cos 2n\phi \right)^2 d\phi \right\} \qquad (3)$$

The first integral in Equation (3) may be put in Fourier series form by use of trigonometric equivalents of the type

$$\cos\phi \sum_{n=1}^{\infty} a_n \sin 2n\phi = \frac{a_1}{2}\sin\phi + \frac{1}{2}\sum_{n=1}^{\infty} (a_n + a_{n+1}) \sin(2n+1)\phi$$

Performing the indicated integrations in Equation (3), it follows that Equation (3) becomes

$$U_1 = \frac{\pi r t E}{2R^2}\left\{ r^2\eta^2 + 3r\eta c_1 + \frac{9}{4} c_1^2 + \frac{1}{4}\sum_{n=1}^{\infty} c_n^2(1-2n)^2 - 2c_n c_{n+1}(2n-1)(2n+3) + c_{n+1}^2 (2n+3)^2 + \frac{\lambda^2}{12}\sum_{n=1}^{\infty} c_n^2(8n^3-2n)^2\right\} \quad (4)$$

where $c_n = a_n = b_n$; $\eta = \Delta\alpha/\alpha$ for in-plane bending.

When internal pressure is considered, the additional work represented by the internal pressure p acting against the change in volume must be considered, per unit length of centerline, this is

$$U_2 = p\Delta A \quad (5)$$

where ΔA = the increase in area of the curved pipe cross-section

$$= \frac{1}{2}\int_0^{2\pi} (r+w_r)^2 d\phi - \frac{1}{2}\int_0^{2\pi} r^2 d\phi$$

$$= \frac{1}{2}\int_0^{2\pi} (2rw_r + w_r^2)\, d\phi \quad (6)$$

The relation $w_r = -dw_t/d\phi$ is derived from the condition of inextensibility, dropping second and higher-order terms. In the case of determining ΔA, however, this is not sufficiently accurate, since the work done by the pressure is itself dependent upon second and higher-order terms in ΔA. Considering second-order terms, it can be shown that

$$\Delta A = -2\pi \sum_{n=1}^{\infty} n^2(4n^2-1)c_n^2 \qquad (7)$$

In order to determine the values of the coefficients c_n, we may differentiate $U = U_1 - U_2$ with respect to each c_n and, by the principle of least work, each of the resulting expressions may be set equal to zero, thereby obtaining

$$\left.\begin{aligned}
\frac{\partial U}{\partial c_1} &= 0 = 3r\eta + (5+6\lambda^2+24\psi)\,c_1 - \tfrac{5}{2}\,c_2 \cdots \\
\frac{\partial U}{\partial c_2} &= 0 = -\tfrac{5}{2}\,c_1 + (17+600\lambda^2+480\psi)c_2 - \tfrac{21}{2}c_3 \cdots \\
\frac{\partial U}{\partial c_n} &= 0 = -c_{n-1}\frac{(2n-3)(2n+1)}{2} + c_n\left\{(4n^2+1)\right. \\
&\qquad \left. +(8n^3-2n)^2\,\frac{\lambda^2}{6} + \left[8n^2(4n^2-1)\right]\psi\right\} \\
&\qquad -c_{n+1}\frac{(2n-1)(2n+3)}{2} \cdots\cdots
\end{aligned}\right\} \quad (8)$$

Equations (8) give a set of n linear equations with (n+1) unknown c's. By assuming that $c_{n+1} = 0$, all constants

may be evaluated. Since the c's all contain a factor of $r\eta$, it is convenient to introduce the relation $d_n = c_n/r\eta$.

The minimized energy U is then equated to work done by the bending moment

$$U_{min} = \frac{1}{2}\frac{M\eta}{R} \tag{9}$$

Flexibility Factor

Substituting the values of $d_n = c_n/r\eta$ from Equations (8) in Equation (9) and solving for η

$$\eta = \frac{RM}{IE}\Big[\, 1+3d_1+\frac{9}{4}d_1^2+\frac{1}{4}\sum_{n=1}^{\infty} d_n^2(1-2n)^2$$

$$-2d_nd_{n+1}(2n-1)(2n+3) + d_{n+1}^2(2n+3)^2$$

$$+\frac{\lambda^2}{12}\sum_{n=1}^{\infty} d_n^2(8n^3-2n)^2+\psi\sum_{n=1}^{\infty} 4n^2(4n^2-1)d_n^2\Big]^{-1} \tag{10}$$

The factor in brackets in Equation (10) is the generalized formula for the flexibility factor K for in-plane bending. It may be simplified to the form

$$K_p = \frac{1}{1+\frac{3}{2}d_1} \tag{11}$$

In the first approximation, for example, with c_2 and higher c_n assumed zero, Equation (8) gives

$$d_1 = \frac{c}{r\eta} = -\frac{3}{5+6\lambda^2+24\psi} \tag{12}$$

and from Equation (11)

$$K_p = \frac{1}{1 - \frac{3}{2}\left(\frac{3}{5 + 6\lambda^2 + 24\psi}\right)} = \frac{5+6\lambda^2+24\psi}{0.5+6\lambda^2+24\psi} \quad (13)$$

When p = 0, Equation (13) reduces to the equations derived by von Karman (in-plane bending). Equation (13), when $p \neq 0$, is confirmed by the work of Kafka and Dunn (10) for in-plane bending by substituting $\nu = 0$ in their equations.

Stresses

The longitudinal strains on which Equations (1) are based are as follows:

$$e_l = \frac{1}{R}\left(\frac{\Delta\alpha}{\alpha} r \sin\phi + w_t \cos\phi + w_r \sin\phi\right) \quad (14)$$

Circumferential strains at the outer and inner-wall surfaces, are given by

$$e_c = \pm \frac{t}{2(1-\nu^2)r^2}\left(\frac{d^3 w_t}{d\phi^3} + \frac{dw_t}{d\phi}\right) \quad (15)$$

The plus sign applies to the outside - wall surface; minus to inside-wall surface.

Strains may be converted to stresses by the usual formulas

$$S_l = \frac{E}{1-\nu^2}\left(e_l + \nu e_c\right) \quad (16)$$

$$S_c = \frac{E}{1-\nu^2}\left(e_c + \nu e_l\right) \quad (17)$$

Combining Equations (14) through (17) along with Equation (2) and noting that η = RMK/IE, the following equations for the stresses are obtained

$$S_l = \frac{K_p Mr}{I(1-\nu^2)}\left[(1+\frac{3d_1}{2})\sin\phi + \frac{1}{2}\sum_{n=1}^{\infty}\left\{d_n(1-2n) + d_{n+1}(2n+3)\right\}\sin(2n+1)\phi \pm \frac{\nu\lambda}{2}\sum_{n=1}^{\infty} d_n(2n-8n^3)\cos 2n\phi\right] \quad (18)$$

$$S_c = \frac{K_p Mr}{I(1-\nu^2)}\left[\pm\frac{\lambda}{2}\sum_{n=1}^{\infty} d_n(2n-8n^3)\cos 2n\phi + \nu(1+\frac{3d_1}{2})\sin\phi + \frac{\nu}{2}\sum_{n=1}^{\infty}\left\{d_n(1-2n) + d_{n+1}(2n+3)\right\}\sin(2n+1)\phi\right] \quad (19)$$

Stress - intensification factors are obtained by dividing Equations (18) and (19) by Mr/I, since these factors are the ratios of the curved - pipe stress to the calculated stress by the ordinary beam theory; which stress is simply Mr/I

Therefore, the longitudinal stress - intensification factor for in-plane bending by a first approximation, from Equation (18), is

$$\frac{S_l}{Mr/I} = \frac{K_p}{1-\nu^2}\left\{\mp 3d_1\nu\lambda\cos 2\phi + (1+\frac{3d_1}{2})\sin\phi - \frac{d_1}{2}\sin 3\phi\right\} \quad (20)$$

The circumferential stress - intensification factor for in-plane bending by a first approximation, from Equation (19), is

$$\frac{S_c}{Mr/I} = \frac{K_p}{1-\nu^2}\left\{\mp 3d_1\lambda\cos 2\phi + \nu\left[\left(1+\frac{3d_1}{2}\right)\sin\phi - \frac{d_1}{2}\sin 3\phi\right]\right\} \qquad (21)$$

It will be apparent, in writing out Equations (11), or (18) and (19), that expressions for the third or fourth-order approximation become quite lengthy and time-consuming to apply. In the case of zero pressure, it was found graphically by Beskin (12) and later shown analytically by Clark and Reissner (3) that, for values of λ less than about 0.3, the flexibility and maximum stress-intensification factors can be expressed by the following simple formulas

$$K = 1.73/\lambda \qquad (22)$$

$$i = 1.95/\lambda^{2/3} \qquad (23)$$

The existence of simple asymptotic formulas for the flexibility and stress - intensification factors without pressure suggested the possibility of similar formulas for these factors with pressure. Values of K_p and i_p were calculated by the series formulas over an appropriate range

of the variables S/E, r/t, and R/r. It was found that by plotting the following

$$\frac{K}{K_p} - 1 \quad \text{and} \quad \frac{i}{i_p} - 1$$

against the variables S/E, r/t, and R/r on logarithmic co-ordinates, that substantially straight-line relations held over the range of these variables likely to be encountered in piping practice; i.e., S/E corresponding to stresses up to 2,800 ksc in steel pipe; r/t up to 50 and R/r from 2 to ∞. These plots then led to the approximate formulas

$$K_p = \frac{K}{1+6\frac{S}{E}\left(\frac{r}{t}\right)^{4/3}\left(\frac{R}{r}\right)^{1/3}} = \frac{K}{1+\frac{S}{E}X_k} \qquad (24)$$

$$i_p = \frac{i}{1+3.25\frac{S}{E}\left(\frac{r}{t}\right)^{3/2}\left(\frac{R}{r}\right)^{2/3}} = \frac{i}{1+\frac{S}{E}X_i} \qquad (25)$$

where

X_k = function of r/t and $R/r = 6\left(\frac{r}{t}\right)^{4/3}\left(\frac{R}{r}\right)^{1/3}$

X_i = function of r/t and $R/r = 3.25\left(\frac{r}{t}\right)^{3/2}\left(\frac{R}{r}\right)^{2/3}$

Note Subtracted from "Effect of Internal Pressure on Flexibility and Stress-Intensification Factors of Curved Pipe or Welding Elbows" by Rodabaugh, E.C. and George, H.H.; ASME Transactions, 1957; Collected papers on Pressure Vessel and Piping Design.

APPENDIX II

STRAIN GAGE TECHNIQUE

Strain gages are used for either of two purposes:-

1. To determine the state of strain existing at a point on a loaded member, for the purpose of stress analysis.
2. To act as a strain-sensitive transducer element calibrated in terms of quantities such as force, pressure displacement, acceleration, etc., for the purpose of measuring the magnitude of the input quantity.

The electrical resistance strain gage is used in this experiment. Theory of operation of this type of gage will be explained herewith. The resistance of an electrical conductor varies according to the following relation

$$R = \frac{\rho L}{A} = \frac{\rho L}{CD^2} \qquad (1)$$

If the conductor is in the state of strain, each variable in Eq. (1) may change. Differentiating Eq. (1) yields

$$dR = \frac{1}{CD^2} (L d\rho + \rho dL) - 2\rho L \frac{dD}{D} \qquad (2)$$

Dividing Eq. (2) by Eq. (1) results in

$$\frac{dR}{R} = \frac{dL}{L} - 2\frac{dD}{D} + \frac{d\rho}{\rho} \qquad (3)$$

which may be arranged in another form as

$$\frac{dR/R}{dL/L} = 1-2\frac{dD/D}{dL/L} + \frac{d\rho/\rho}{dL/L} \qquad (4)$$

Let $e_l = dL/L$ = longitudinal strain cm./cm.

$e_c = dD/D$ = circumferential strain cm./cm.

μ = Poisson's ratio = $\frac{-dD/D}{dL/L}$

$F = \frac{dR/R}{dL/L}$ = gage factor

Therefore

$$F = \frac{dR/R}{dL/L} = \frac{dR/R}{e_l}$$

$$= 1 + 2\mu + \frac{d\rho/\rho}{dL/L} \qquad (5)$$

Rewriting Eq. (5) and replacing the differential by an incremental resistance change, the following equation is obtained

$$e = \frac{1}{F}\frac{\Delta R}{R} \qquad (6)$$

This is the fundamental procedure for using resistance strain gages. In practical application, values of F and R are supplied by the gage manufacturer, and we determine ΔR corresponding to the input situation intended to measure. In this experiment Tinsley Telcon strain gages type W8/120/G/K/2 are used. The gage factor is 1.92 and gage resistance is in the ranges between 120.7 ~ 121.7 ohms.

The surface of the test specimen around which the strain gages were stuck had to be mechanically ground with an electric grinder to remove any traces of rust and scale. Then it was smoothly rubbed by grade zero emery cloth and finally cleaned and polished by cleansing fluid such as carbontetrachloride or acetone. To stick the gage, a thin layer of Durofix adhesive was first coated on the surface and allowed to dry out. A second layer of cement was then applied and the gage attached at the position and excess adhesive were squeezed out by pressure of the thumb. After the attachment of sixteen gages are completed, they were left to dry for at least 48 hours. A thin layer of vaseline was required over the gages to prevent them from moisture. Then the gages were wired up to strain gage bridge, dummy gage and selector switch to form a D.C. Wheatstone Bridge circuit as shown in FigA11 and A13. The strain gage bridge diagram was shown in Fig.A12. The voltage of the battery was always checked to see whether the pointer of the meter reached the red line. If not, the recharge was needed. The gage factor dial was set to 1.92 as specified by the manufacturer. The initial reading of every gage was obtained by pressing the detector button and recorded the value of measuring dial that brought the pointer to the zero

position. When loaded, the measuring dial was also adjusted until the pointer was at zero position and the value recorded. The difference was the required percent strain. If "pull for $\frac{1}{10}$" button was pulled, the required percent strain had to be divided by 10. For the bridge used herein, the percent strain in the ranges of -0.1 to 0.1 % and -1 to 1 % could be measured.

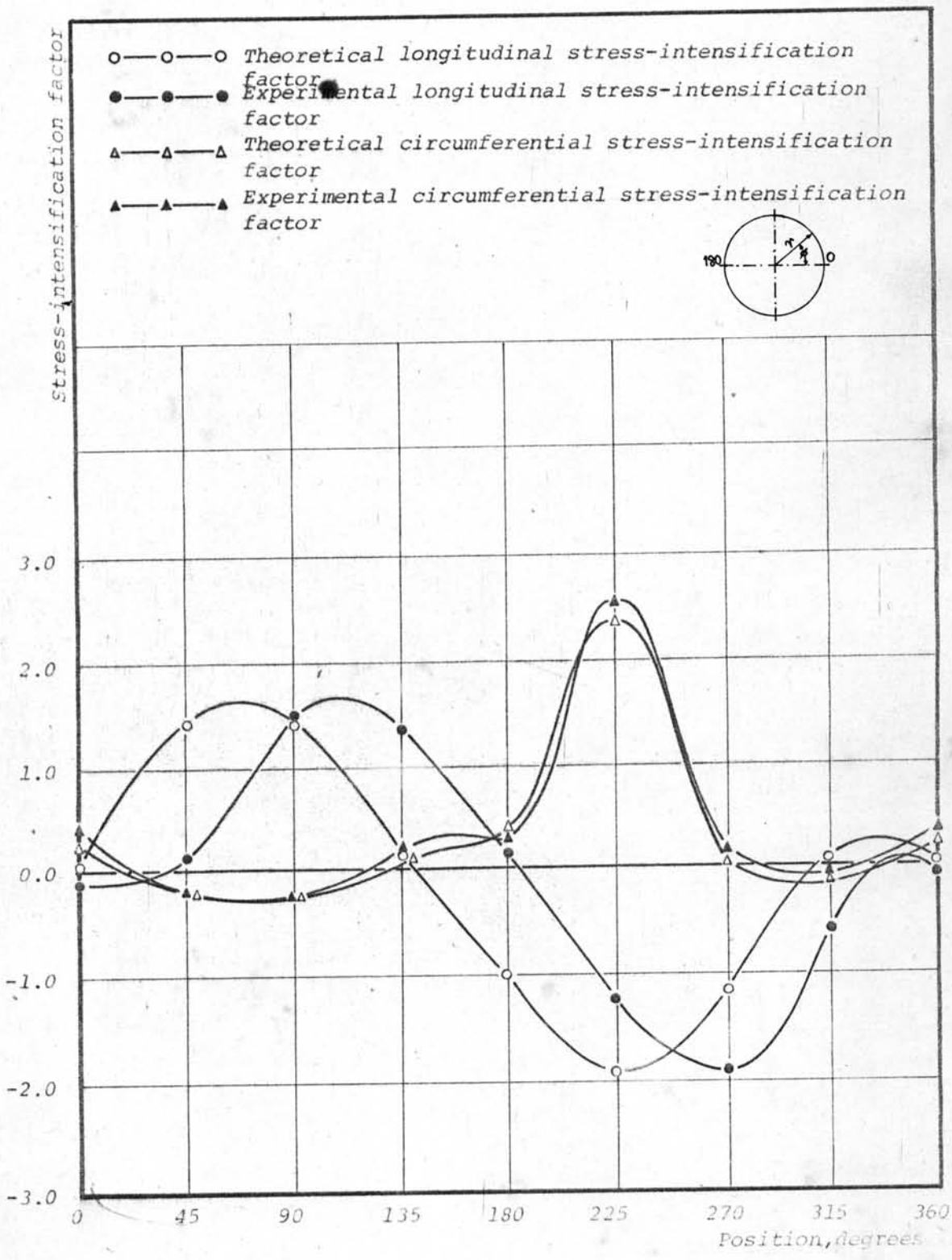

Fig.A1. Comparison between theoretical and experimental longitudinal and circumferential stress-intensification factor(p = 10ksc, F = 1,000 kg.)

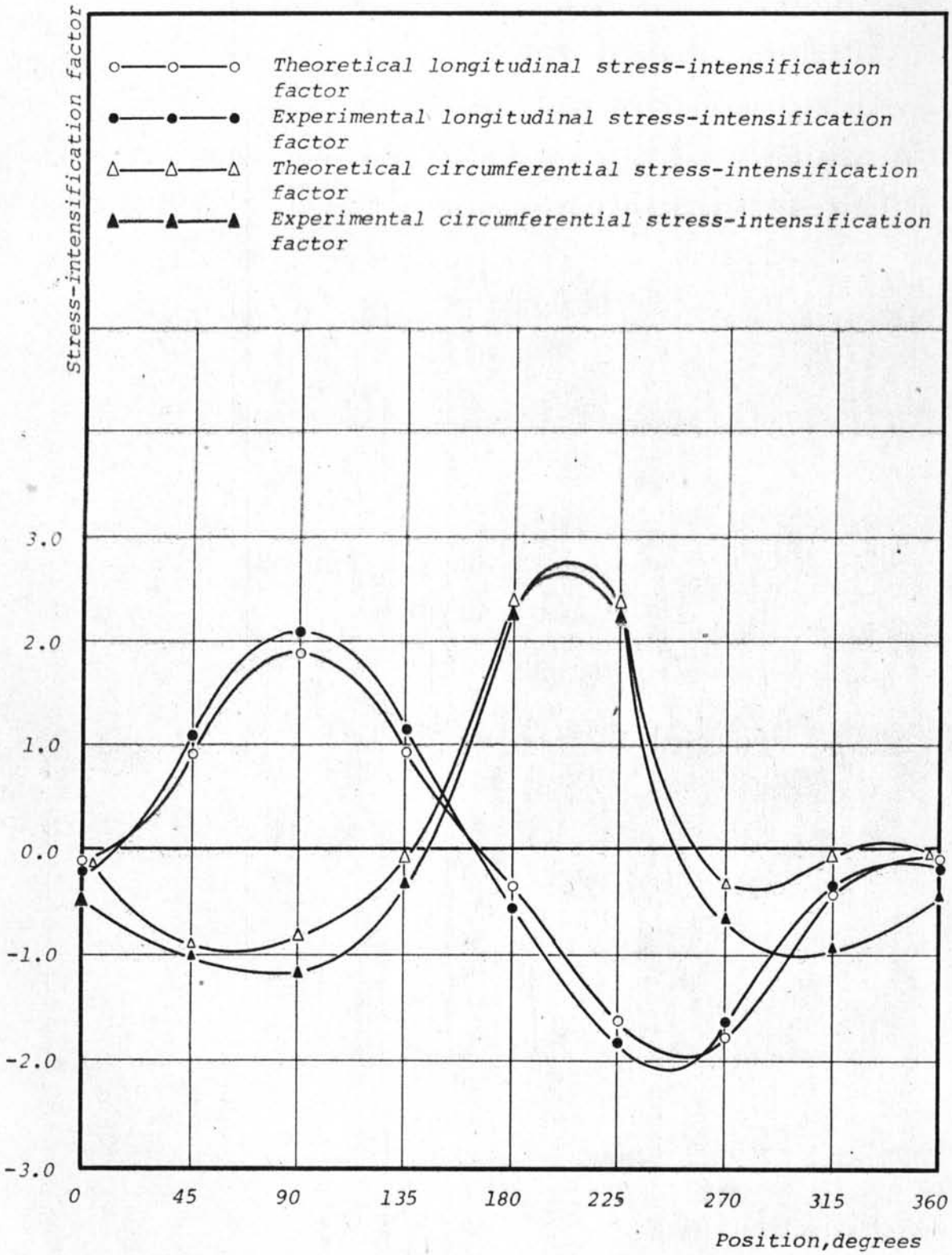

Fig.A2. Comparison between theoretical and experimental longitudinal and circumferential stress-intensification factor (p = 10 ksc., F = 2,000 kg.)

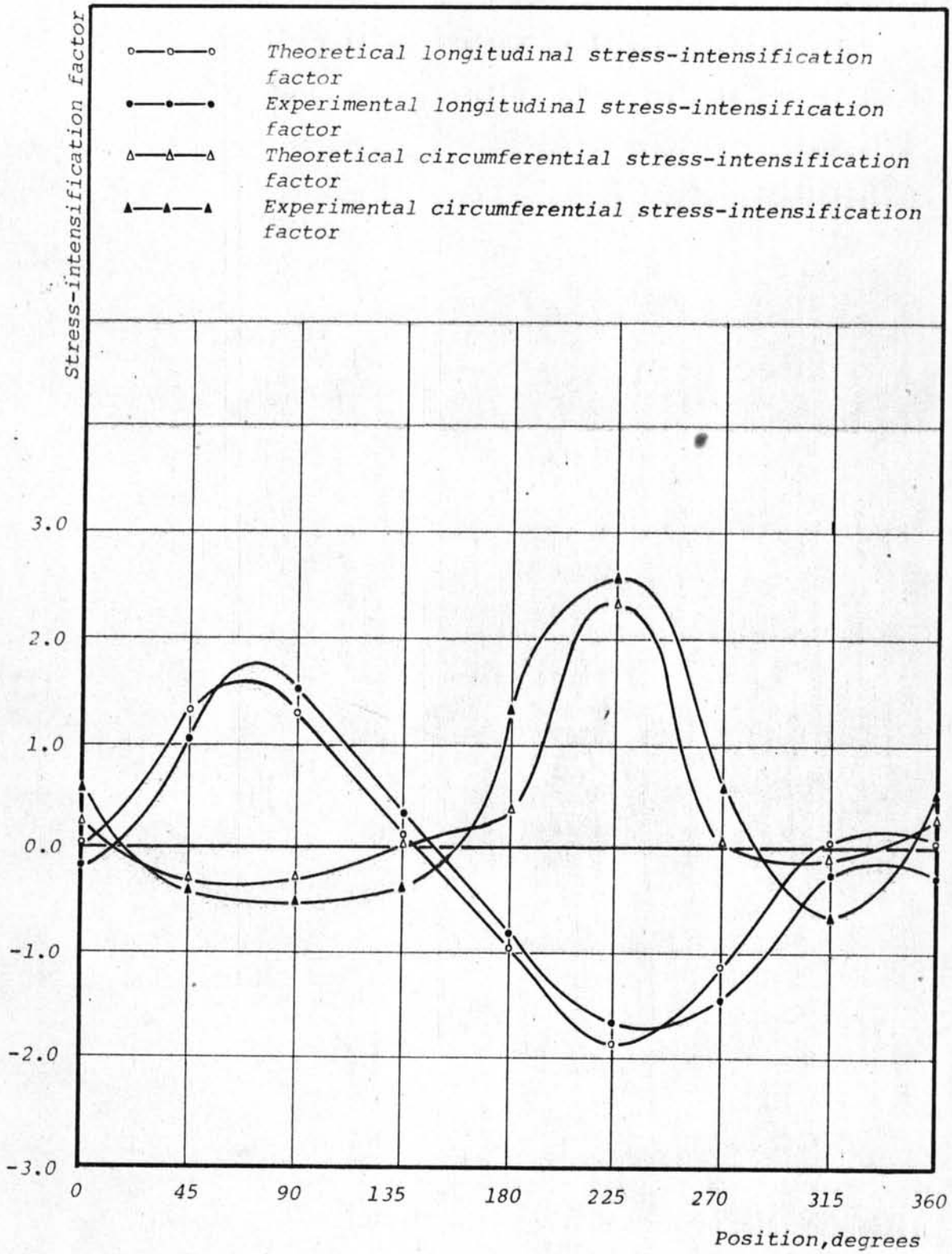

Fig.A3. Comparision between theoretical and experimental longitudinal and circumferential stress-intensification factor (p = 20 ksc., F = 1,000 kg.)

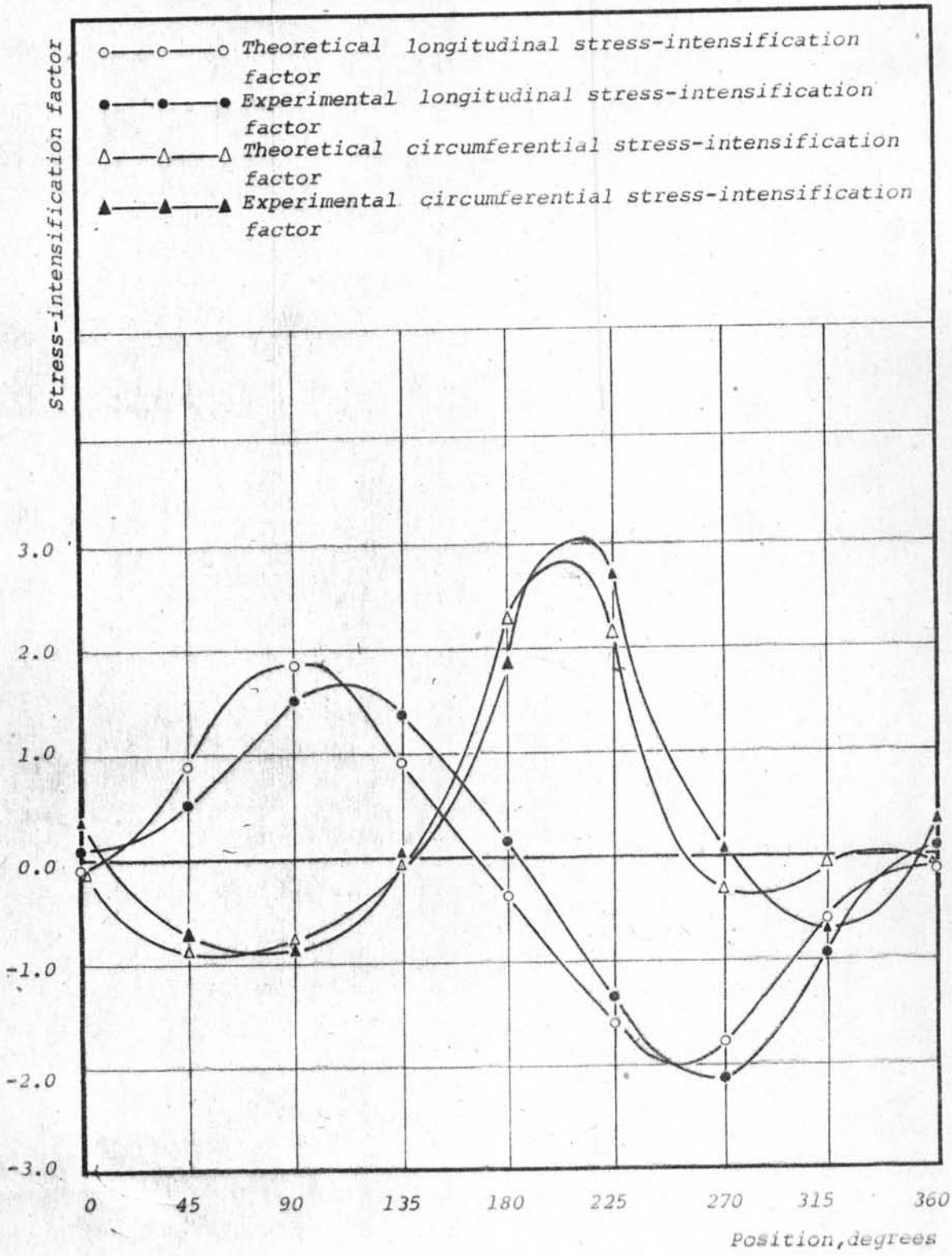

Fig.A4. Comparison between theoretical and experimental longitudinal and circumferential stress-intensification factor (p = 20 ksc., F = 2,000 kg.)

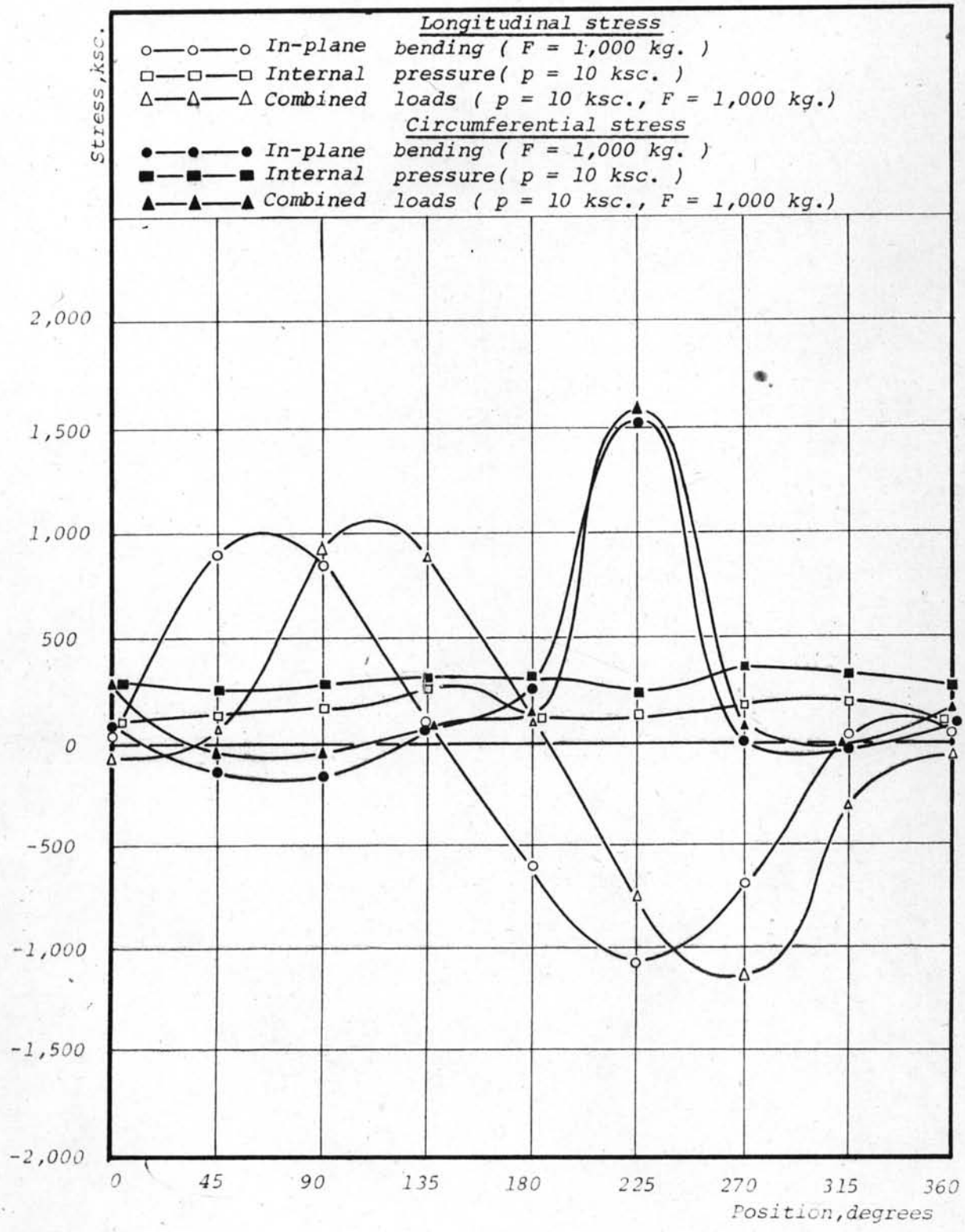

Fig.A5. Variation of longitudinal and circumferential stresses around the pipe cross-section under various types of load.

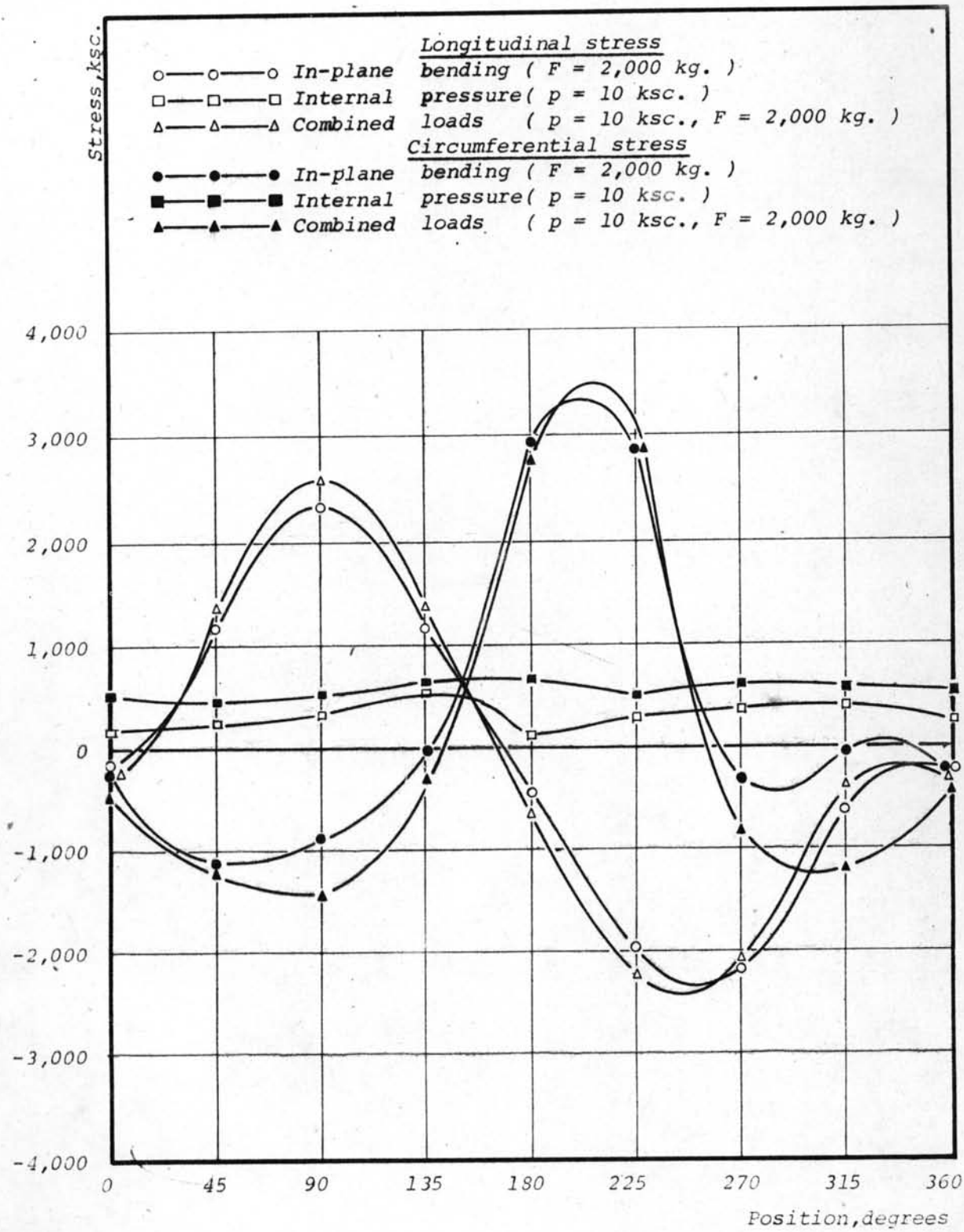

Fig.A6. Variation of longitudinal and circumferential stress around the pipe cross-section under various types of load.

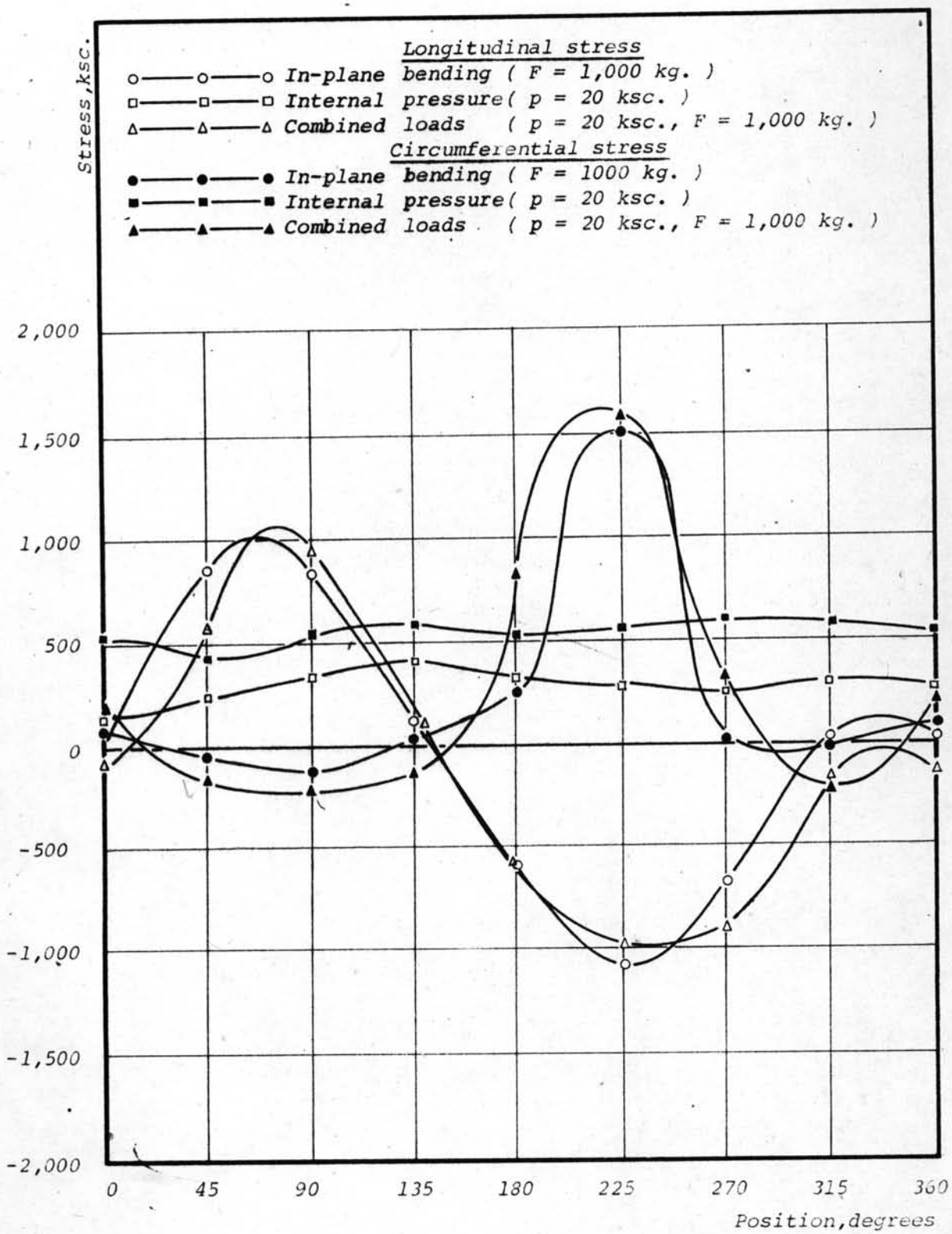

Fig.A7. Variation of longitudinal and circumferential stress around the pipe cross-section under various types of load.

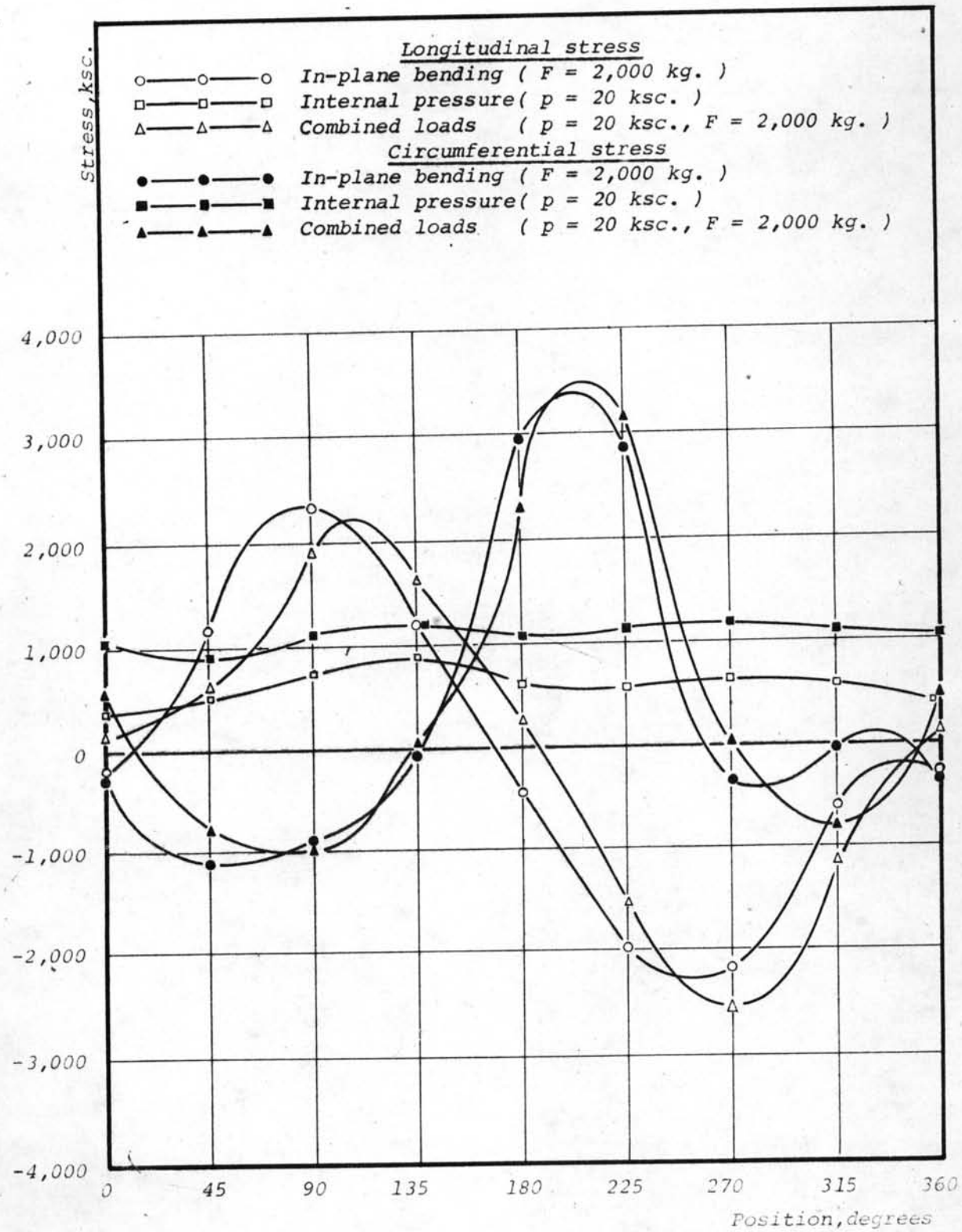

Fig.A8. Variation of longitudinal and circumferential stress around the pipe cross-section under various types of load.

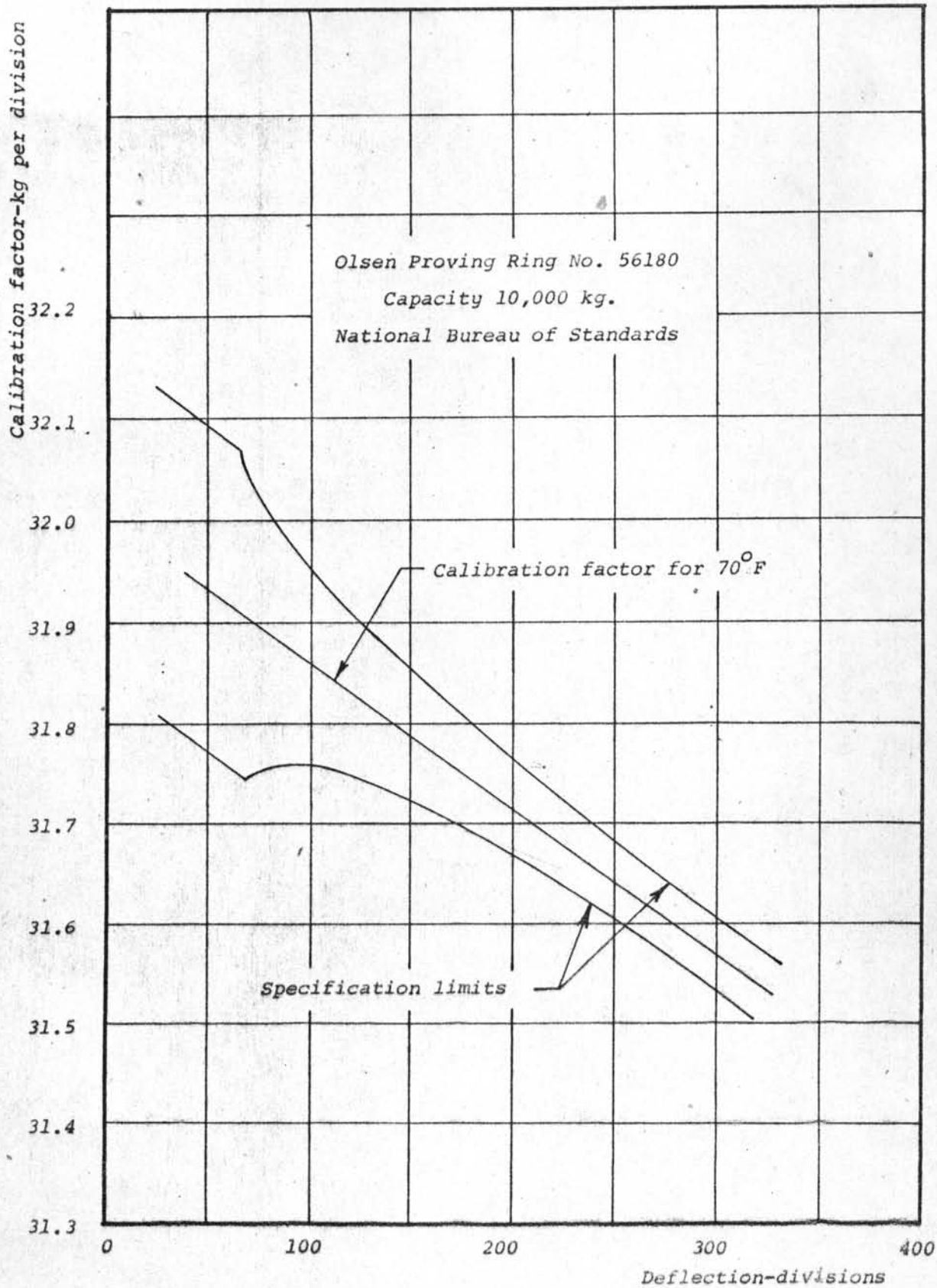

Fig.A9. Calibration curve of Proving Ring No. 56180

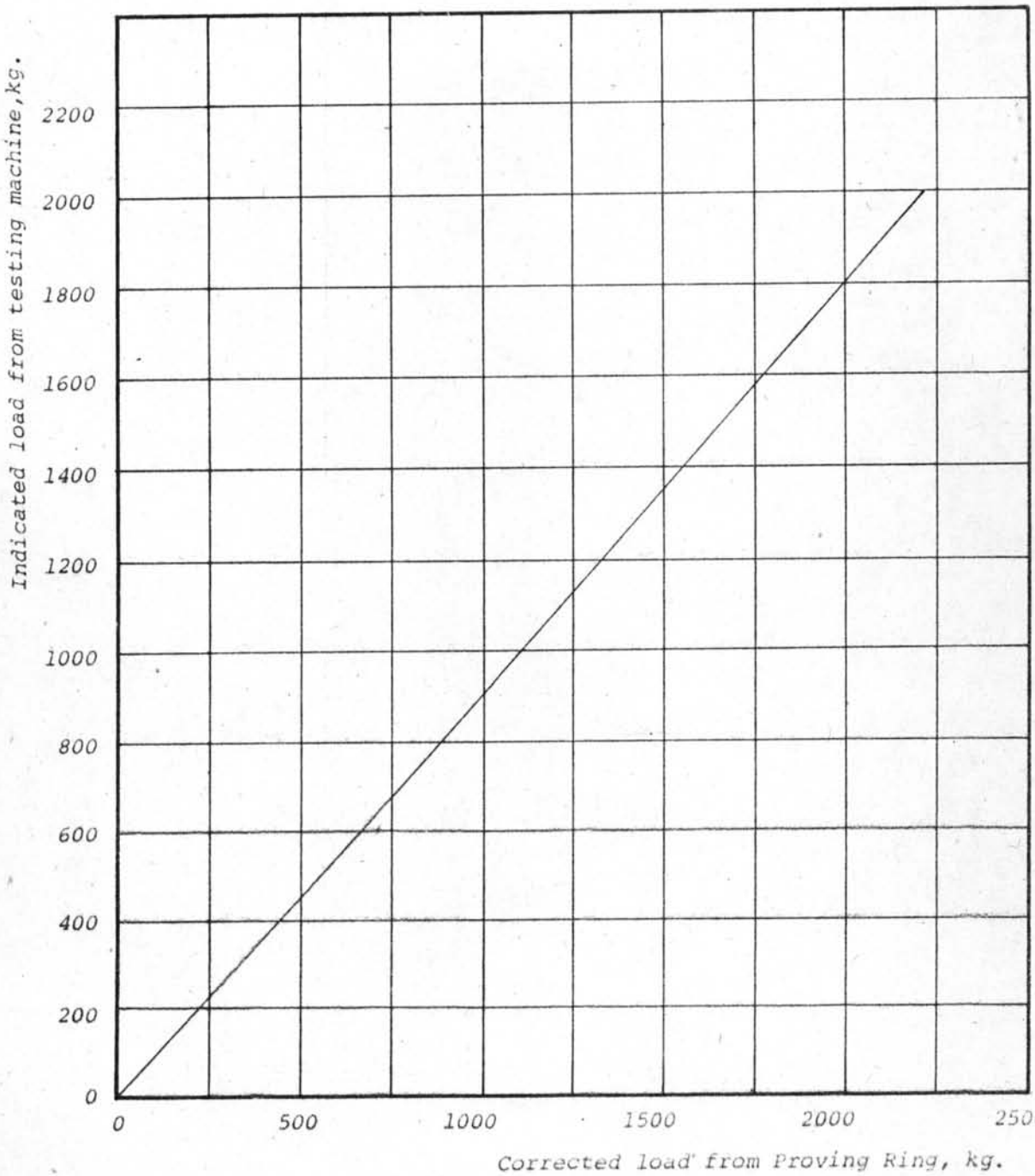

Fig.A10. Calibration curve of AMSLER TESTING MACHINE No. 060355AK
Capacity 20 tons, load range 0 ~ 2 tons.

Note :- When used with external Apex Unit open Link between terminals 2 and 3

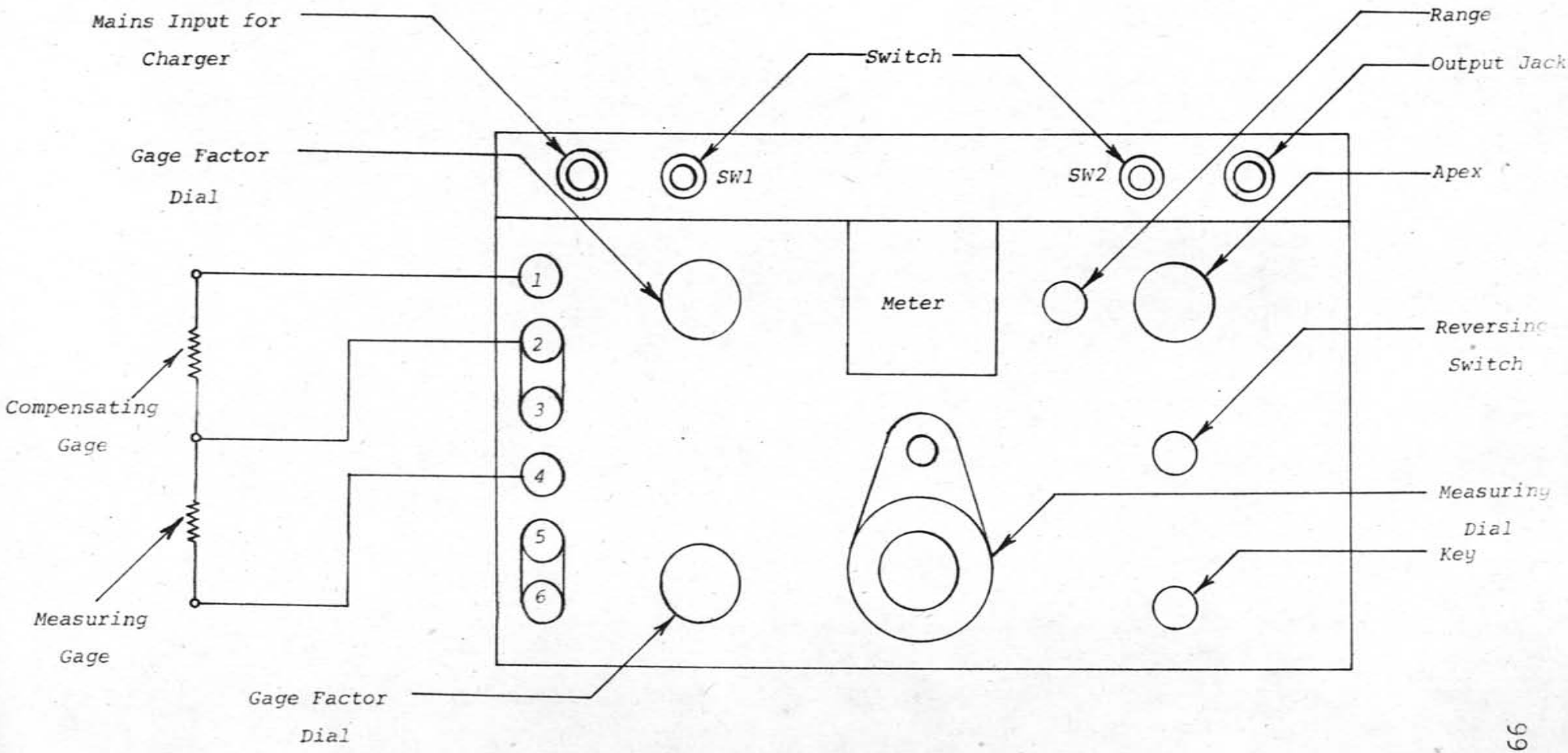

Fig.All. Strain gage bridge connections for two arm bridge

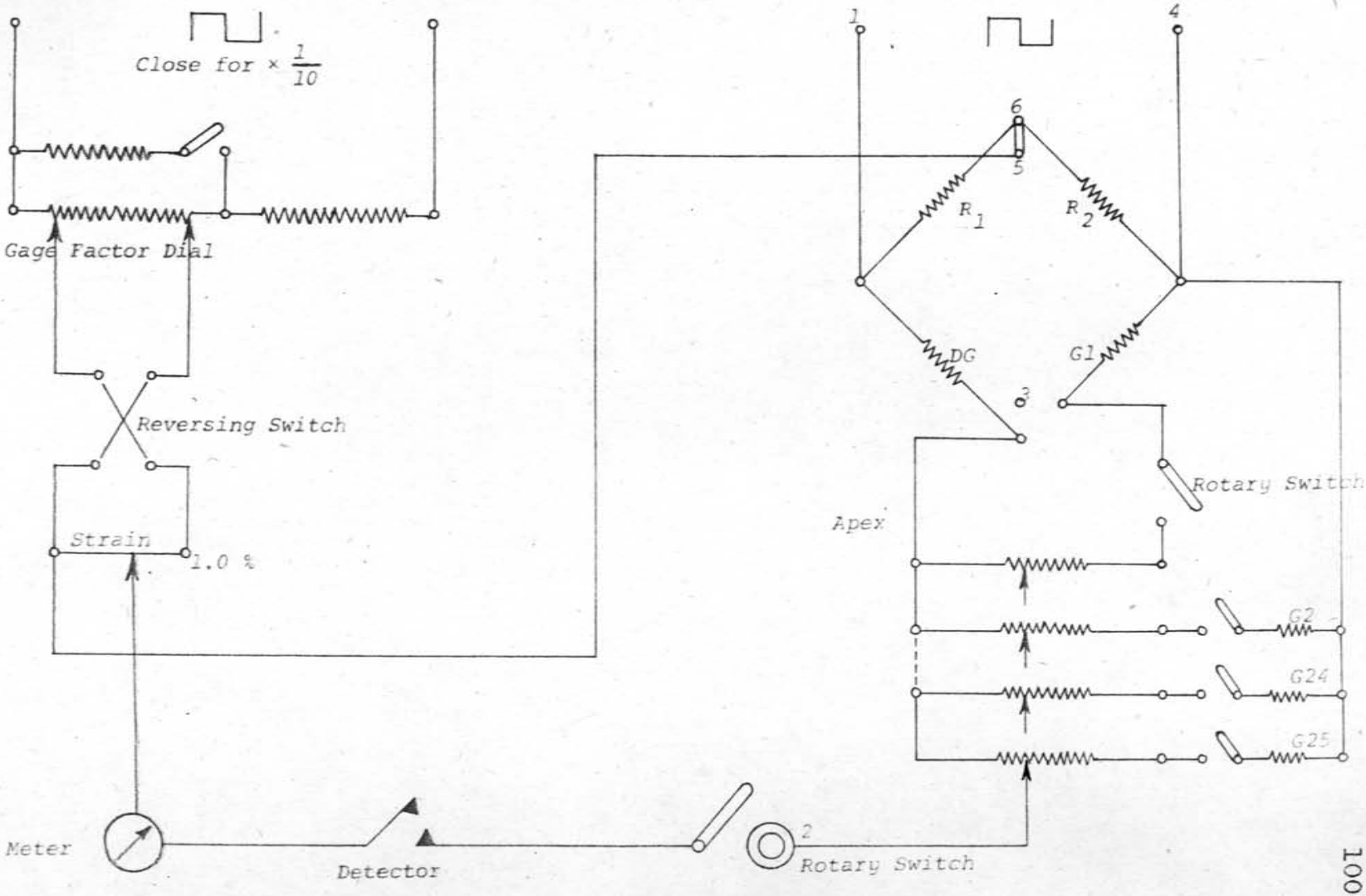

Fig.A12. Strain Gage Bridge Diagram

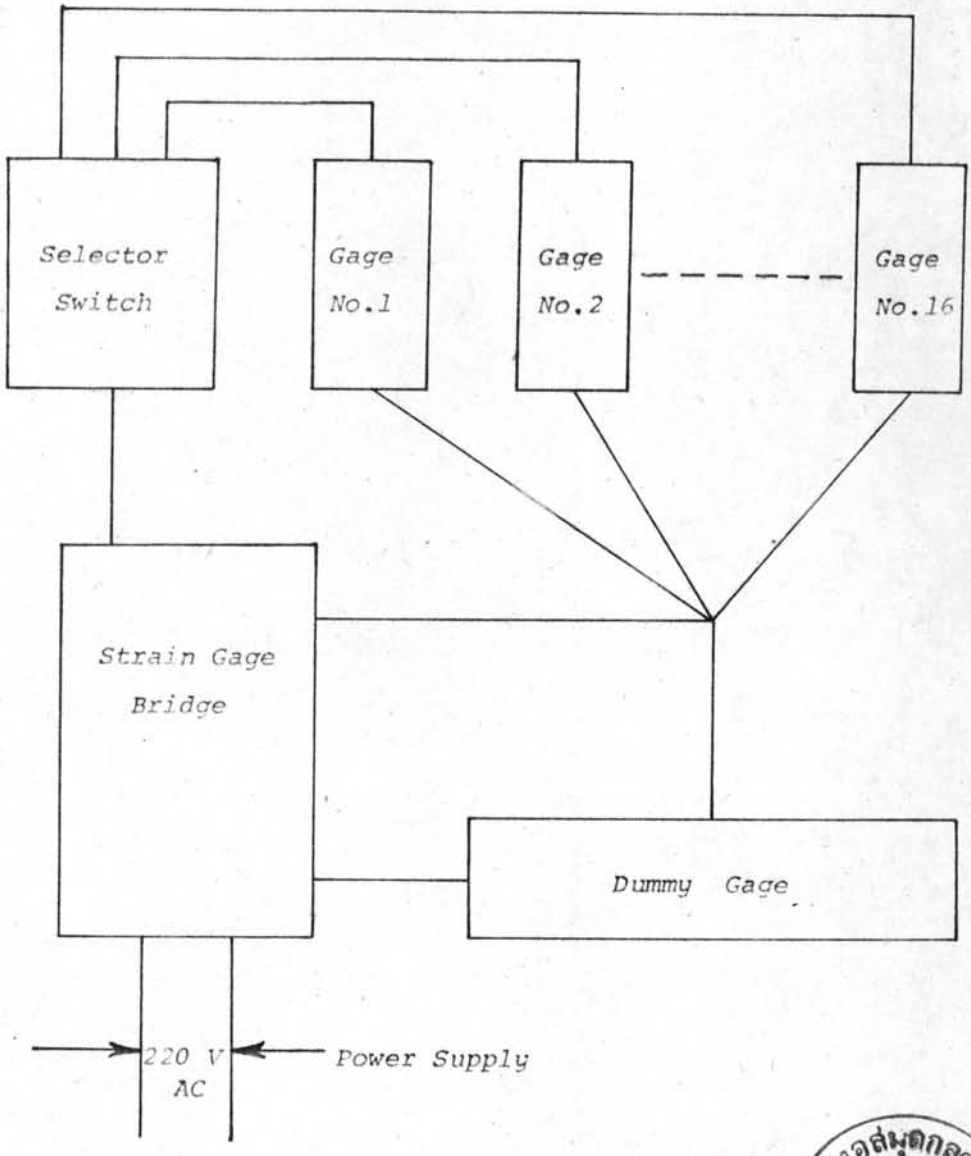

Fig.A13. Schematic diagram of strain measurement

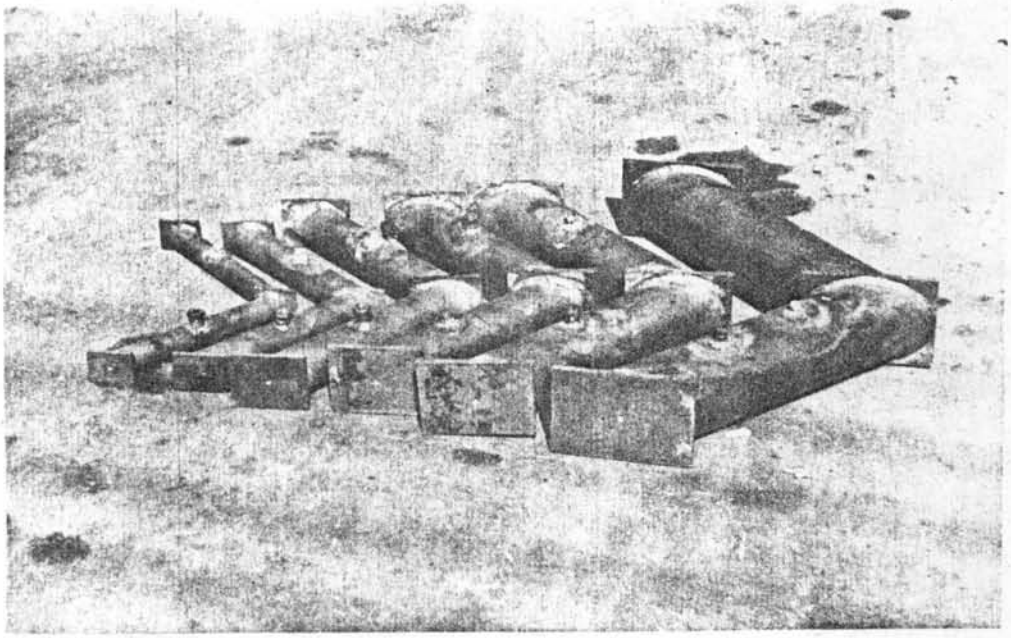

a) Reinforced single mitered pipe bend

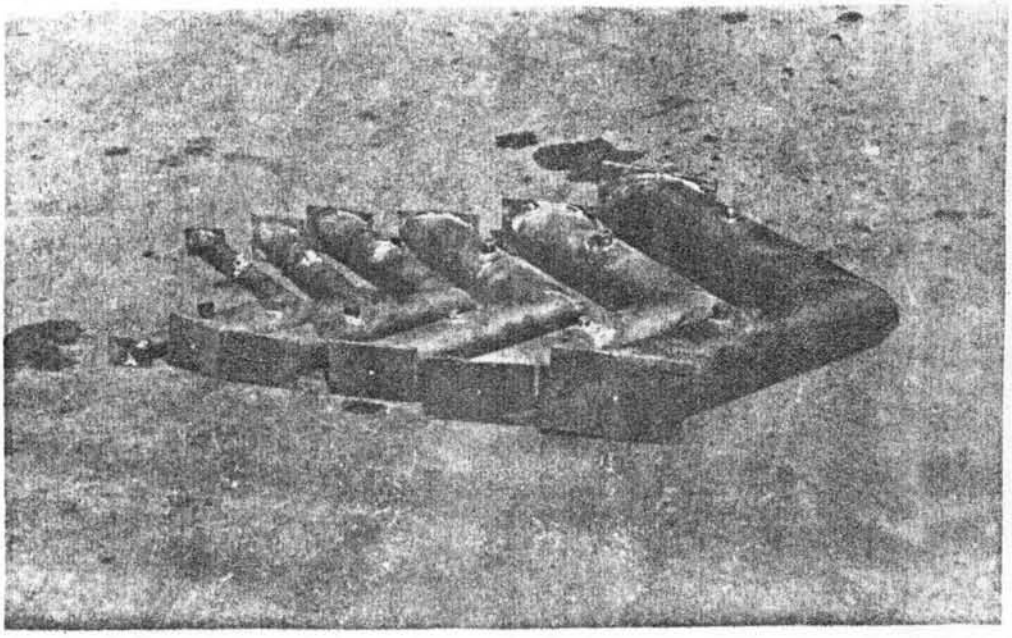

b) Unreinforced single mitered pipe bend

Fig.A14. Single mitered pipe bend

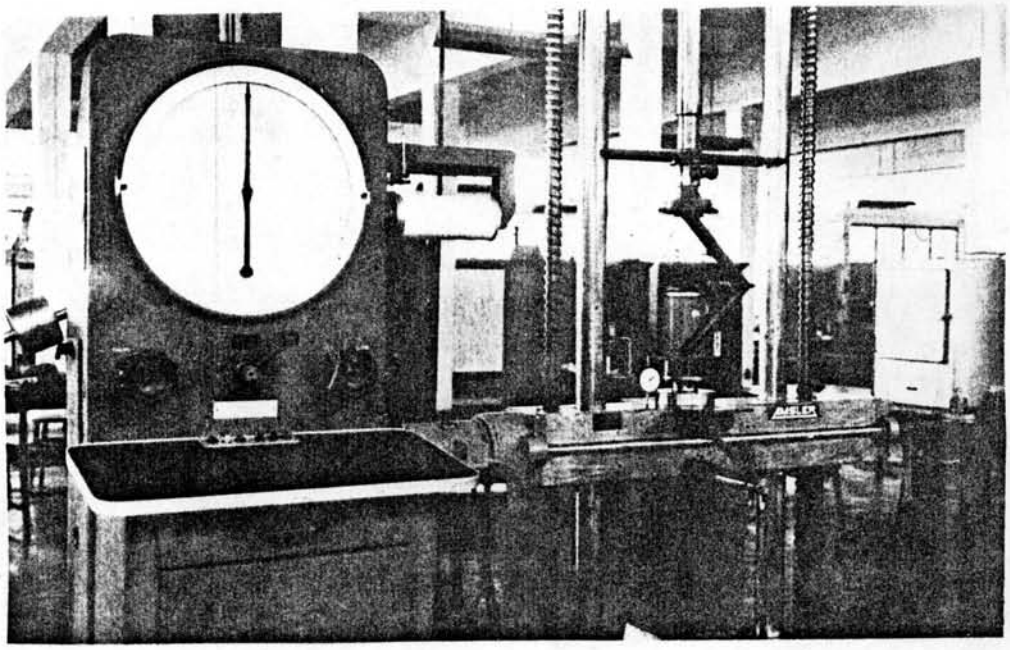

Fig.A15. Amsler Universal Testing Machine

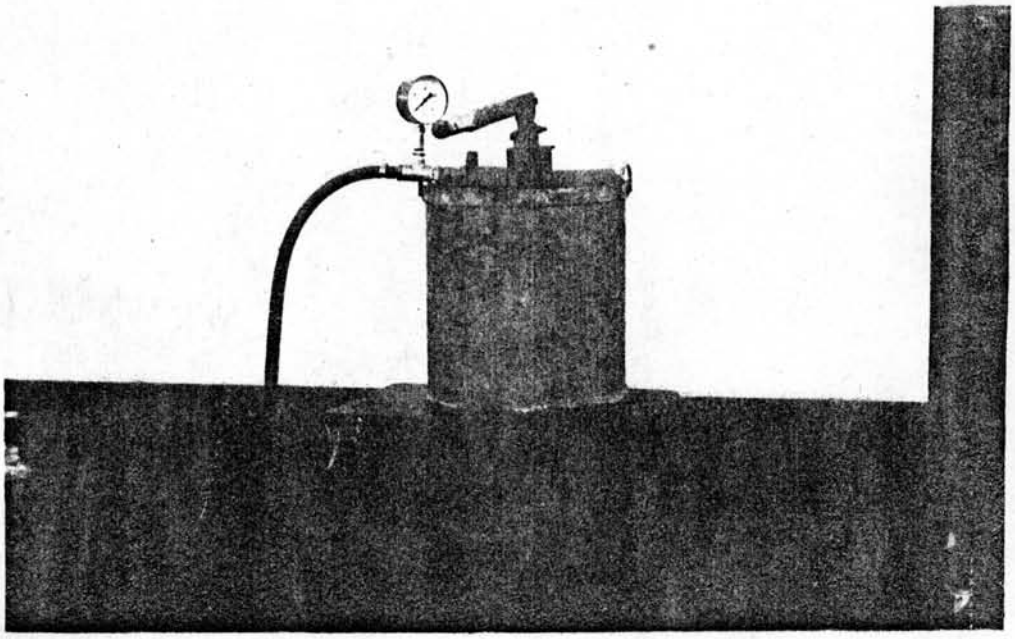

Fig.A16. Hand pump

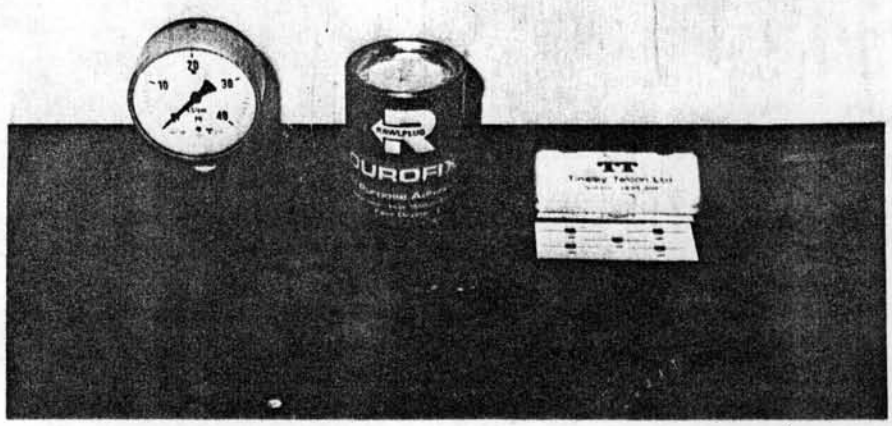

Fig.A17. Strain gage and cement, Pressure gage

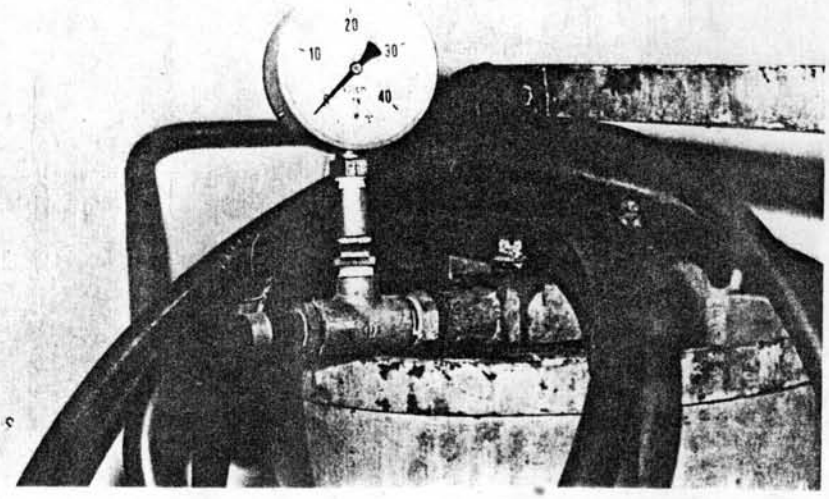

Fig.A18. Reducers and flexible pipe

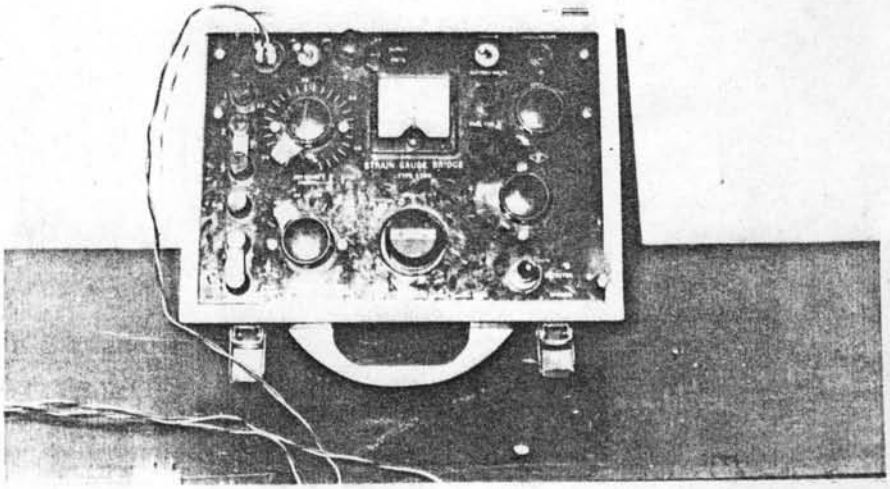

Fig.A19. Strain gage bridge

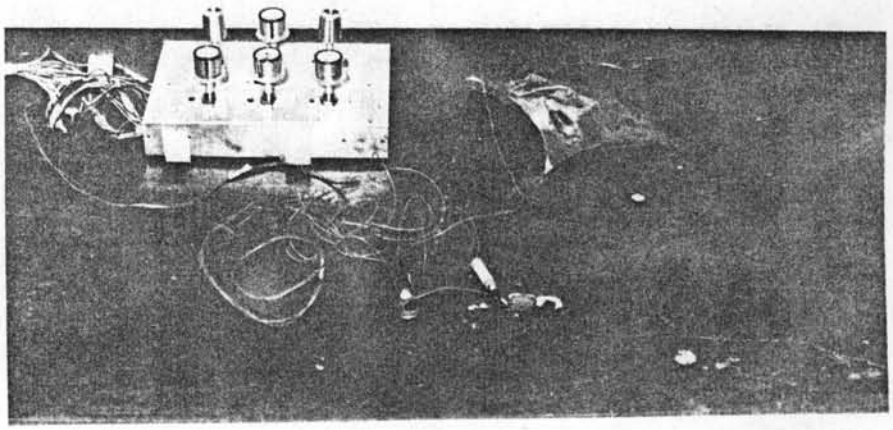

Fig.A20. Selector switch and dummy gage

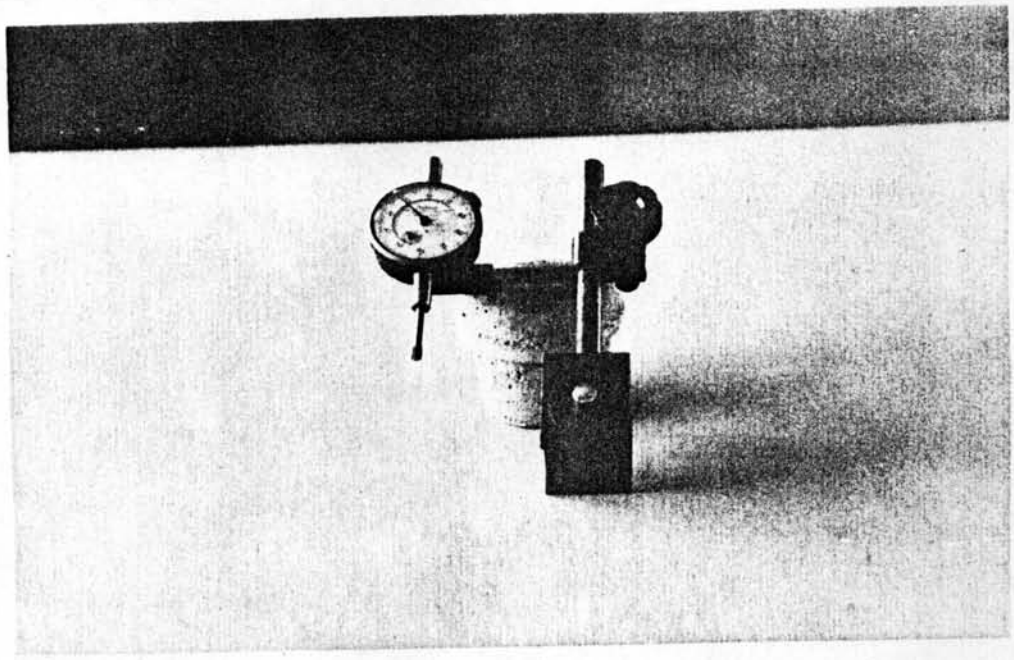

Fig.A21. Dial gage with magnetic holder

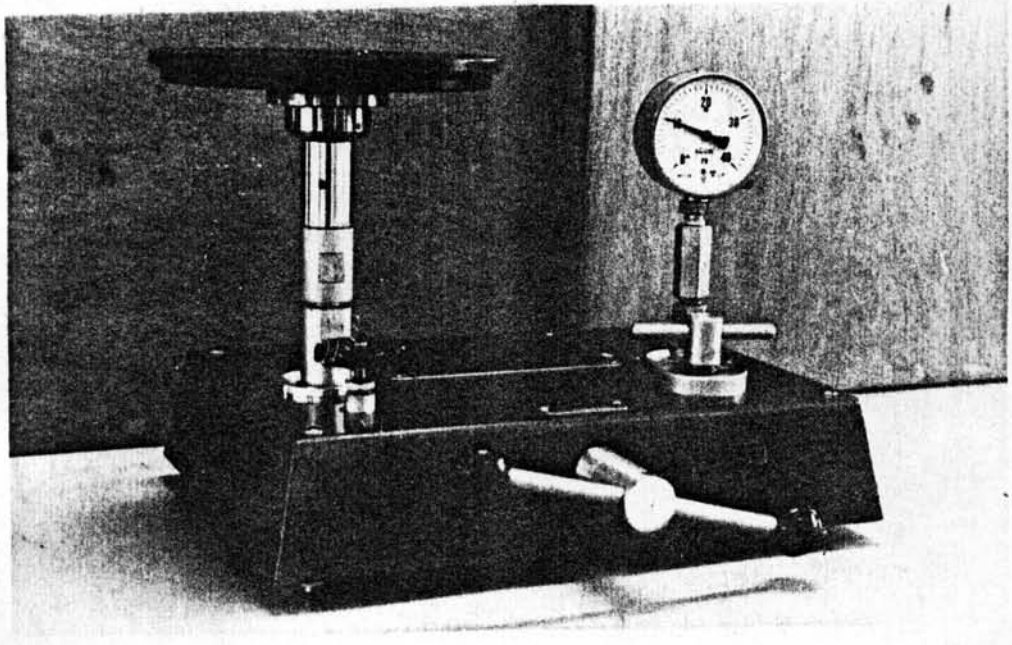

Fig.A22. Calibration of pressure gage

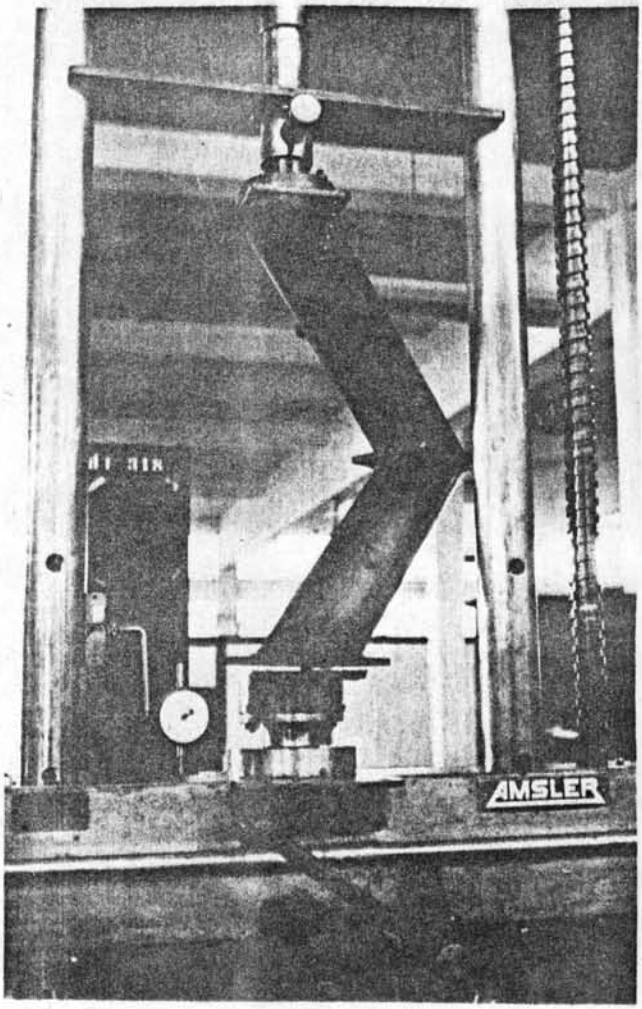

Fig.A23. Flexibility under pure in-plane bending

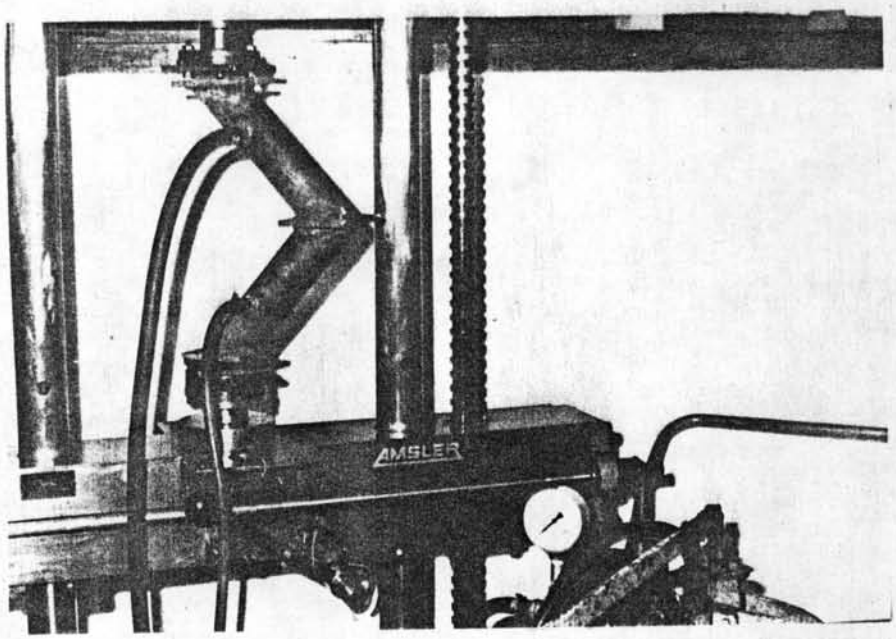

Fig.A24. Flexibility under combined pressure and in-plane bending load

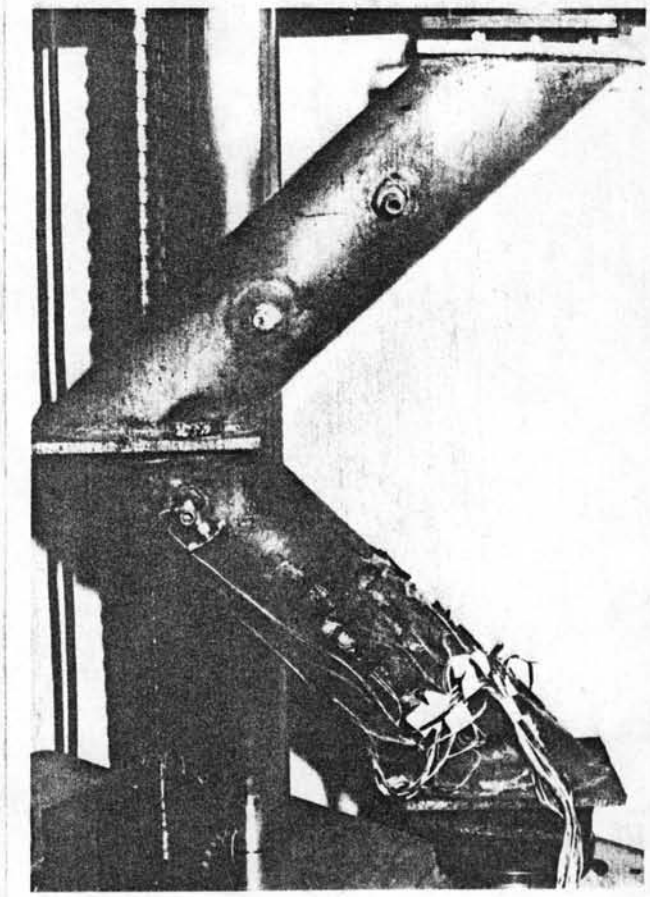

Fig.A25. Pipe specimen with completely attached strain gages

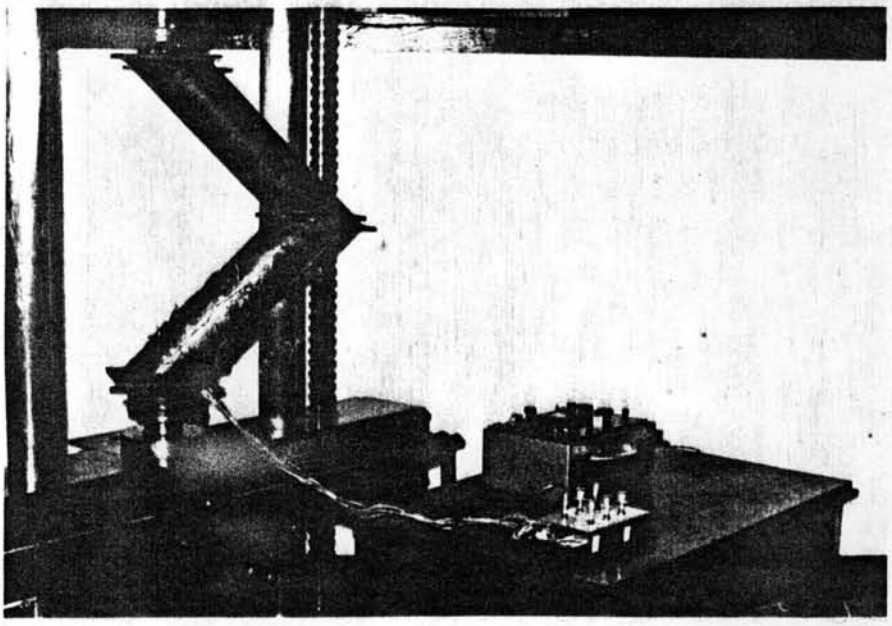

Fig.A26. Strains of the pipe subjected to in-plane bending

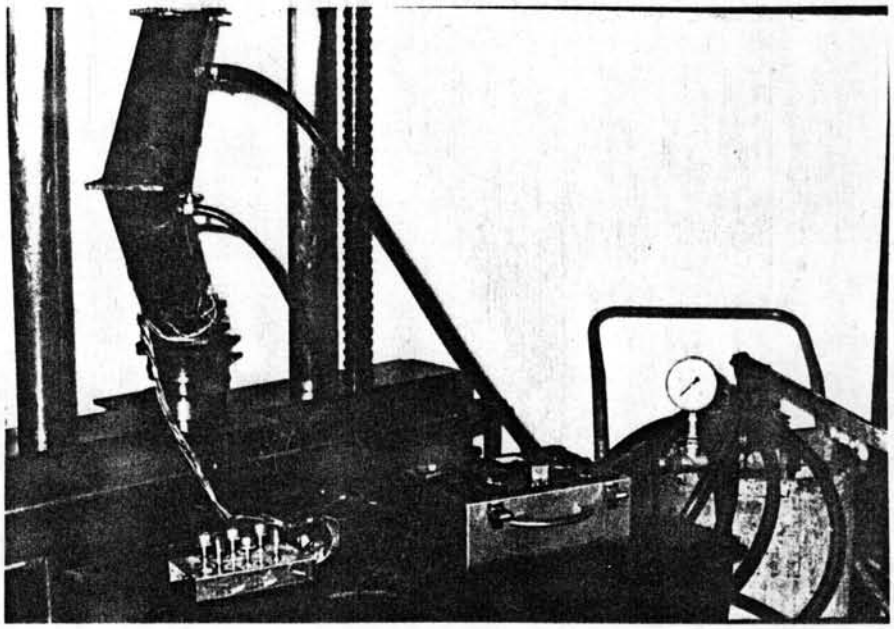

Fig.A27. Strains of the pipe subjected to combined load